



July 2020 heavy rainfall in Japan: effect of real-time river discharge on ocean circulation based on a coupled river-ocean model

Yu-Lin K. Chang¹ · Sergey M. Varlamov¹ · Xinyu Guo^{1,2} · Toru Miyama¹ · Yasumasa Miyazawa¹

Received: 1 November 2022 / Accepted: 4 April 2023 / Published online: 26 April 2023
© The Author(s) 2023

Abstract

In July 2020, a stationary atmospheric front over Japan caused persistent, nearly continuous rain for most of the month that resulted in new historical highest rainfall records in several areas and caused serious river floods, landslides, and debris-flow events. An existing hindcast and forecast ocean circulation model that includes climatological discharge information of major rivers failed to represent the extreme river discharge under heavy rainfall. New experiments were conducted using real-time river discharge information based on Today's Earth CaMa-Flood simulation that includes 368 rivers in Japan. The inclusion of real-time river discharge improved the salinity bias in the near-surface waters. The differences were significant compared to the observations in the heavy rain region (i.e., Ariake Bay and Tosa Bay), and insignificant at offshore stations. The ensemble experiments of real-time river discharge cases suggested the difference between the climatological and the real-time river discharge experiments was not random, but was robust. The freshening water changed the shelf circulation, and its far-reaching effect appeared hundreds of kilometers away from the shore. Passive particle tracking was conducted for examining the cross-shelf exchange. More particles released from Bungo Channel went offshore in near-surface water when the real-time river discharge was used compared to using the climatology discharge. Particles released in Tosa Bay, Seto Inland Sea, and Kii Channel showed the opposite tendency. The real-time river discharge not only changed the modeled coastal salinity distribution, but also the coastal and offshore currents. The role of the real-time river discharge on modeling normal flow periods or drought events, and its influence on a longer time scale model simulation remain to be explored.

Keywords River discharge · Extreme rainfall · Ocean modeling

1 Introduction

In July 2020, a stationary atmospheric front formed in East Asia, extending from China to the east of Japan (Zhao et al. 2021). The front stayed above Japan for nearly a month, which brought warm and humid air towards Japan, resulting in persistent heavy rainfall. The front first hit southern and western Japan, starting on 3 July. The continuous rain resulted in the historical maximum rainfall record in Kyushu of 496 mm in 24 h. After that, with a minor shifting

in position, it stayed above Japan until 28 July. The 1-month of rain led to hazards, such as floods, landslides, and mud flows that resulted in a loss of 84 lives, and thousands of houses were destroyed (<https://www.data.jma.go.jp/obd/stats/data/bosai/report/2020/20200811/20200811.html>). The heavy rainfall also induced 1–2 cm crustal subsidence in the flooded region, which was recovered after the water drained into the ocean (Heki and Arief 2022).

The heavy rain not only influenced the terrestrial areas of Japan, but it also affected the ocean. Freshwater discharges, however, are often neglected in global climate models, because the scale of the atmosphere and ocean are much greater than the rivers (Miller et al. 1994). Global rivers carry more than one-third of land-based precipitation to the ocean (Trenberth et al. 2007). The buoyant freshwater affects the coastal dynamics as it merges with deeper and saltier ocean water, and the materials carried by the rivers also influence coastal ecosystems (Horner-Devine et al. 2015). The river plumes are mostly directed offshore and then turn

Responsible Editor: Fanghua Xu

✉ Yu-Lin K. Chang
ychang@jamstec.go.jp

¹ Application Laboratory, Japan Agency for Marine-Earth Science and Technology, Yokohama 236-0001, Japan

² Center for Marine Environmental Studies, Ehime University, Matsuyama 790-8577, Japan

to form shore-parallel coastal currents that are driven by the Earth's rotation and centrifugal acceleration (Garvine 1987). In estuaries, dense shelf water flows into the estuary below the outflowing fresher surface layer. This bidirectional flow is the estuarine circulation, sometimes called the exchange flow (Geyer and MacCready 2014). Although river discharge occurs locally, it could affect coastal circulation by changing offshore salinity and therefore density (Dai et al. 2009). The near-surface currents could be modified by river-induced momentum flux and turbulence (Carniel et al. 2009). High-volume river discharge from large rivers or due to extreme rainfall can not only affect the coastal region, but also has a nonnegligible far-reaching effects (Urakawa et al. 2015). A recent study investigated the 2018 July heavy rain event in the Seto Inland Sea and found that the 4-day rainfall caused a long-lasting change in temperature and salinity in Bungo Channel and therefore modified the circulation and enhanced the cross-shelf exchange between the Seto Inland Sea and the Pacific Ocean for about 2 months (Morimoto et al. 2022). In July 2020, there was more precipitation and it lasted longer than during the 2018 event in the same region, so the cross-shelf exchange between the Seto Inland Sea and Pacific Ocean via the Bungo Channel and Kii Channel might also be modified.

A high-resolution ocean hindcast and forecast system has been used to monitor the seas around Japan (JCOPE-T DA, (Miyazawa et al. 2021)) since it came online in 2019 (https://www.eorc.jaxa.jp/tree/ocean_model/index.html). JCOPE-T DA has the most updated satellite information assimilated and is expected to provide coastal prediction information during heavy rain periods. Although JCOPE-T DA did include the freshwater discharge, its river discharge input was based on monthly climatology, which was likely unable to reproduce the actual coastal circulation condition due to the overestimation and/or underestimation of short-term river discharge. Similar to JCOPE-T DA, monthly climatological river runoff was also used in other major ocean models, such as the Ocean General Circulation Model for the Earth Simulator OFES (Sasaki et al. 2020) and Global Reanalysis Hybrid Coordinate Ocean Model HYCOM (Chassignet et al. 2009), due to the limited access to real-time river information.

Underestimates of river discharge often occurred during the typhoon season. A previous study investigated the coastal salinity variation from two selected typhoons (Troselj et al. 2017). They ran an offline river runoff model based on the observed rainfall data and made an optimized parameterization for deriving the best-fit river discharge. The modeled river discharge was then used in the ocean model, which changed the near-coast salinity distributions compared to when the climatological river discharge was used. However, they did not describe details of the oceanic conditions affected by the extreme river discharge together

with quantitative validation using in-situ salinity data. A similar method that introduced the river discharge data from the river runoff model to the ocean model was also applied by Urakawa et al. (2015). Instead of focusing on an extreme weather condition, they presented the long-term mean condition. They suggested that the case with river discharge helped to reduce the coastal salinity error compared to the case without river input. Extreme precipitation events have occurred more frequently in Japan in recent years because of the warming of air and ocean temperatures, as well as atmospheric moisture stability near Japan (Kawase et al. 2020). Therefore, a more accurate river discharge dataset is needed to replace the long-used monthly climatology river discharge data.

The objective of this study was to improve the ability to accurately simulate the coastal salinity and currents during heavy rain periods. We introduced real-time hourly river discharge from a river routing model into JCOPE-T DA for simulating the July 2020 heavy rain event in the southwestern Japan region. How the coastal and offshore salinity changed with a shift from monthly climatology river discharge to using the real-time hourly river discharge was investigated. Changes of salinity and coastal currents, as well as their far-reaching effects are presented. Changes in cross-shelf exchange in heavy rain regions are shown based on the particle tracking method.

2 Data and methods

2.1 Observation data

Salinity data collected from various sources was used for comparing to the model performance under different sources of river discharge input. Salinity was measured by CTD casts from ships or fixed recording locations at a total of 36 stations during the target period of July 2020. Salinity data at the mouth of Ise Bay (Fig. 1, red dot) was obtained from the Ise Bay environmental database (<http://www.isewan-db.go.jp/>), and it was recorded by a bottom-mounted tower that provided near surface (~ 3 m), and subsurface (around 15 m and 25 m depth) information. Data at Kojima and Nagahama in Ariake Bay in Kyushu (Fig. 1 magenta dots) were recorded from buoys at the sea surface, and was provided by the Fisheries Research Center of Kumamoto Prefecture. Ship observations were available in Tosa Bay (Fig. 1, blue dots) and offshore Japan (Fig. 1, green dots). Salinity in Tosa Bay was observed by the ship Tosa-Kaiyo Maru, and the data was provided by the Fisheries Center of Kochi Prefecture. Data for offshore Japan was provided by the Japan Coast Guard. Since the fresh and low-density river discharge was mainly distributed in the

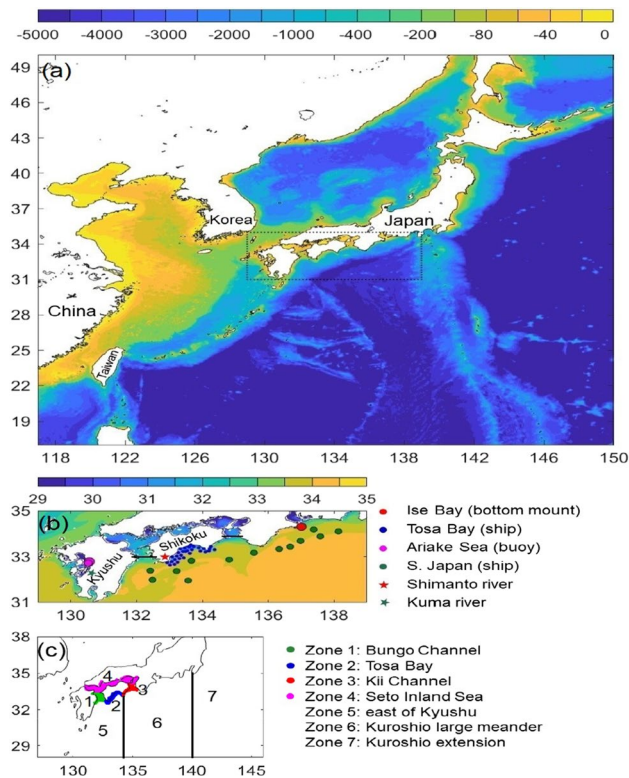


Fig. 1 **a** Ocean bathymetry in the western North Pacific Ocean for the model domain. The region in the black dotted box was enlarged in **(b)**. **b** The climatology salinity in July and the locations for salinity observations: bottom-mounted tower at Ise bay (red dot), buoys in the Kojima and Nagahama in Ariake Sea in Kyushu (magenta dots), ship observations in Tosa Bay (blue dots) and off southern Japan (green dots), selected rivers: Shimanto River (red star) and Kuma River (green star) used in Fig. 2, and the sections used for computing transport in Fig. 9. **c** Particle tracking release map. Color represents different release regions: Bungo Channel (zone 1, green), Tosa Bay (zone 2, blue), Kii Channel (zone 3, red), and Seto Inland Sea (zone 4, magenta)

shallow water, the near-surface (depth ≤ 10 m) observed salinity data were used.

Satellite-observed gridded Multi-Mission Optically Interpolated Sea Surface Salinity (OISSS) from NASA was used to compare the general performance of the model simulation. OISSS has a 0.25-degree resolution, and the time interval is 4 days. Note that the salinity data used were not assimilated into the hindcast runs, and they are thus considered independent from the simulation results.

3 Real-time river discharge

The river discharge output from the river routing model (CaMa-Flood; (Yamazaki et al., 2011)) operated by Japan Aerospace Exploration Agency was used in the present study. CaMa-Flood was a gridded model with $1/60^\circ$ (~ 2 km

horizontal resolution. The domain covered East Asia from 123°E to 148°E , and from 24 to 46°N , which included Japan, Korea, and part of China. The hourly data was available from September 2018 to the present. CaMa-Flood model received input from the weather reanalysis of the Japan Meteorological Agency and satellite land information. Based on the calculated runoff amounts, CaMa-Flood solved the local inertial equation and enabled hydrodynamic simulation within the river and over the floodplain. The CaMa-Flood river discharge output was validated against observations, which had a reasonable correlation coefficient of 0.55 among all Japanese rivers for the period between 2010 and 2015 (Yoshimura et al., 2008; Ma et al., 2021). The freshwater discharge at the river mouth used in the ocean model included both the river discharge and floodplain flow. The floodplain flow was generally smaller than river discharge. It accounted for less than 5% of total discharge without rainfall, but could increase to 25–35% of total discharge during heavy rain periods. 368 rivers in Japan were included from the CaMa Flood model. Two of the largest rivers, the Shimanto River in Shikoku and the Kuma River in Kyushu were selected for showing the discharge difference between monthly climatology and real-time discharge.

4 The general ocean circulation model

The ocean circulation model used for this study was based on the tide-resolving data-assimilative nowcast and forecast system (JCOPE-T DA; (Miyazawa et al. 2021)). JCOPE-T DA was constructed from the Princeton Ocean Model (Blumberg and Mellor 1987) with a generalized coordinate system (Miyazawa et al. 2009). The model domain encompassed East Asia (17 – 50°N and 117 – 150°E), with a horizontal resolution of $1/36^\circ$ (~ 3 km) and 46 vertical layers. The external forcing to drive the model included wind stresses and net heat/freshwater fluxes at the sea surface converted from the hourly atmospheric reanalysis and forecast produced by the Global Forecast System (GFS) of the National Centers for Environmental Prediction (NCEP). Satellite and in situ temperature and salinity data were assimilated into the model based on a multi-scale three-dimension variational method (Miyazawa et al. 2017). The tidal components were provided by the $1/12$ -degree Oregon State University Tidal Inversion Software OTIS, (Egbert and Erofeeva 2002). The freshwater discharge from the land was represented as water volume fluxes at river mouth grids with monthly mean climatological discharge volumes (Varlamov et al. 2015). The monthly climatology included 108 rivers in Japan and 43 rivers in China, Korea, Taiwan, and Russia. The operational JCOPE-T DA had an initial run in June 2018. It allowed daily and hourly output and could cover a 3-weeks maximum forecast. The restart files were kept every 7 days based on

storage-volume constraints. Comparison between observational data and JCOPE-T DA was performed in a previous study (Miyazawa et al. 2021), which showed satisfactory performance in simulating the three-dimensional circulation over the western North Pacific Ocean.

The hindcast result of JCOPE-T DA served as the initial condition for the river discharge experiments in the present study. The initial date for the experiments was set on 27 June 2020 when the restart file became available. Two experiments were conducted: (1) the river discharge used the default monthly climatology (Exp. Clim), (2) the river discharge used the hourly real-time CaMa Flood (Exp. CamaF) data. The two experiments restarted from the same initial condition, then ran freely until 31 July 2020 when the heavy rain ended. Apart from the river discharge, all other parameters were identical among the experiments. Note that the CaMa Flood model had a smaller domain than the model, so that only the river discharges in Japan were used, and the climatology discharge remained in use outside of Japan. Therefore, this study focused on the variation near Japan where input sources of rivers were different, and especially on the heavy rain region near Shikoku and Kyushu. Hourly data was used for the analyses shown below. Daily data was used for sensitivity experiments that are shown in the discussion.

5 Ensemble simulation experiments

Ensemble experiments were conducted to examine the reliability of Exp. CamaF. Eight ensemble experiments were set up by perturbing their initial conditions in Exp. CamaF. The perturbed initial conditions were simply extracted from daily snapshot model conditions of 7, 12, 17, 22 June, and 2, 7, 12, 17 July 2020, which were close to the starting time of 27 June 2020. Apart from the initial conditions, all other settings in the ensemble experiments remained identical to Exp. CamaF.

6 Particle tracking scheme

The passive particle-tracking method was used to investigate the cross-shelf exchange in the heavy rain region near Shikoku. The two model experiments described above provided the background hourly ocean current. The tracking scheme was based on the fourth-order Runge–Kutta method (Press et al. 1992) with a tracking time step of 1 h. The vertical motion was not included in this study, and particles were tracked horizontally. Two experiments were conducted that both released particles in 4 zones surrounding Shikoku (Fig. 1c). The first experiment released particles at depth of 5 m in the heavy rain region near Shikoku. The second experiment released particles at the same horizontal

locations, but at depth of 50 m. The particles were released in hourly intervals from 00:00 to 23:00 on 1 July 2020 to account for different tidal phases, and were tracked at the fixed depths until 31 July 2020 after the heavy rain ended. Particles were released in a 2-km horizontal interval and about 88,000 particles were released in each experiment. Note that if particles encountered local water depths shallower than the assigned water depth, in order to avoid hitting the sea floor, particles would then be tracked at 90% of water depth.

For sensitivity experiments, particle tracking based on daily-mean data was conducted. Particles were released at the same locations and depths as described above and also tracked for the same period. The tracking results based on daily-mean data were presented in the discussion. The significance of the difference between the experiments was assessed using the chi-square test.

7 Results

The largest river discharge occurred in June, July, or August depending on the region based on the monthly climatology. The overall July average discharge in the Shimanto River is $327 \text{ m}^3/\text{s}$, but in 2020, the real-time discharge went beyond the long-term mean from 3 July when heavy rain started and even exceeded $2000 \text{ m}^3/\text{s}$ on 4, 6, and 10 July (Fig. 2, blue). A relatively dry period occurred between 15 and 23 July before the next rain arrived. Similarly, the heavy rain also resulted in extraordinary maximum discharge of over $5000 \text{ m}^3/\text{s}$ in the Kuma River in Kyushu, whereas its climatological July average was $355 \text{ m}^3/\text{s}$. The monthly averaged real-time discharge in July 2020 was $690 \text{ m}^3/\text{s}$ and $765 \text{ m}^3/\text{s}$ for Shimanto and Kuma rivers, respectively. During July 2020, the real-time discharge had an excessive total volume of $1.23 \times 10^6 \text{ m}^3$ from all targeted rivers in Japan that was

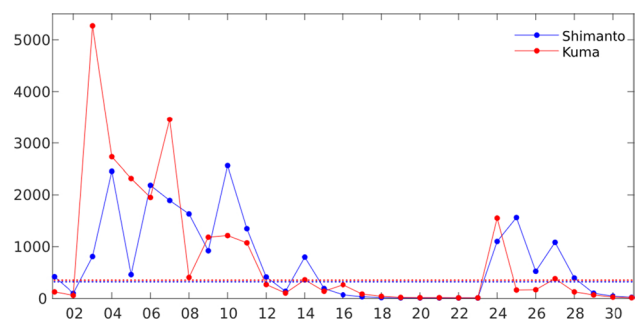


Fig. 2 River discharge (m^3/s) in July 2020 for the Shimanto River in southwestern Shikoku (blue) and the Kuma River that flows into the Ariake Sea in western Kyushu (red). Dotted lines showed the climatological average river discharges in July (not daily data). Note that the values in 18–23 July were small but non-zero

significantly larger than the total climatological discharges of $0.42 \times 10^6 \text{ m}^3$.

The salinity in the heavy rain regions from the two model experiments was compared against the observations. Both model experiments captured the major sea surface salinity pattern, showing higher salinities in the Japan Sea and North Pacific and lower values north of Kyushu and east of Hokkaido (Fig. 3a–c). The salinity bias showed a lower salinity; hence, there was a greater negative bias in Exp. CamaF in comparison to Exp. Clim (Fig. 3d, c). The satellite image, however, did not cover the shallow water region; therefore, it was difficult to judge if real-time discharge improved or degraded the accuracy of coastal salinity by comparing against satellite data alone. To examine salinity change in the coastal region, the in-situ observations were examined next. The salinity around 3 m depth in Ise Bay was about 30–31 before the heavy rain started on 3 July and then it gradually dropped with the cumulative rains and reached its minimum of around 21 on 13 July before returning to 30–32 in a week (Fig. 4a). Both modeled salinities showed a positive bias. Salinity in Exp. Clim showed a weak variation, with salinity being changed by the freshwater input by less than 3. Exp. CamaF improved from Exp. Clim by showing a maximum salinity decrease of 6, although the decrease in salinity was still smaller than the observations. Exp. CamaF resulted in a smaller root-mean-squared error (RMSE) of 4.52 in comparison to the 5.58 value of Exp. Clim, yet the difference between the two experiments was not significant at the Ise Bay station ($p > 0.1$).

Salinity in Ariake Bay was observed at the sea surface, and the model simulation also showed a general positive bias

Fig. 3 Sea surface salinity on 17 July 2020 based on **a** satellite OISSS, **b** Exp. Clim, **c** Exp. CamaF, and **d** the bias and standard deviation error between satellite OISSS and Exp. Clim (black) and Exp. CamaF (red) during July 2020

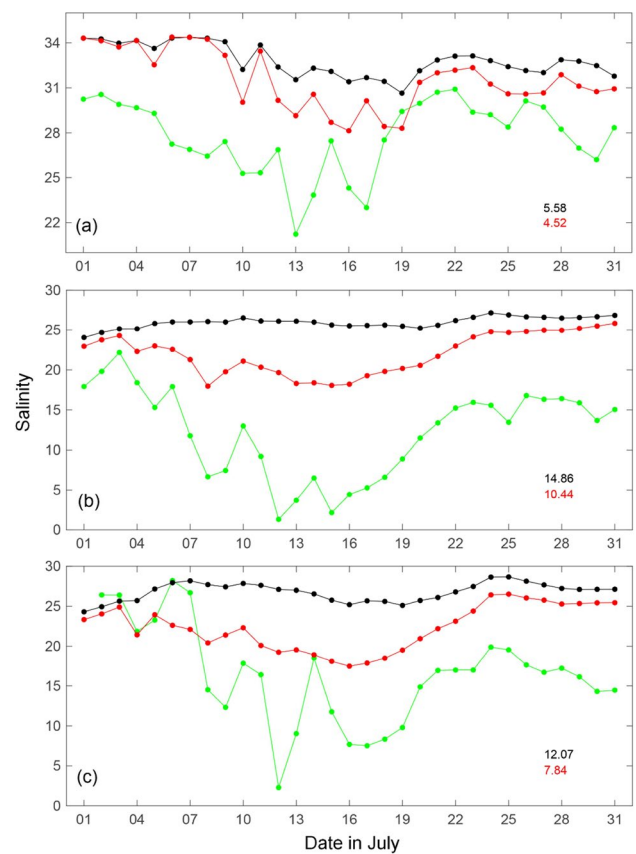
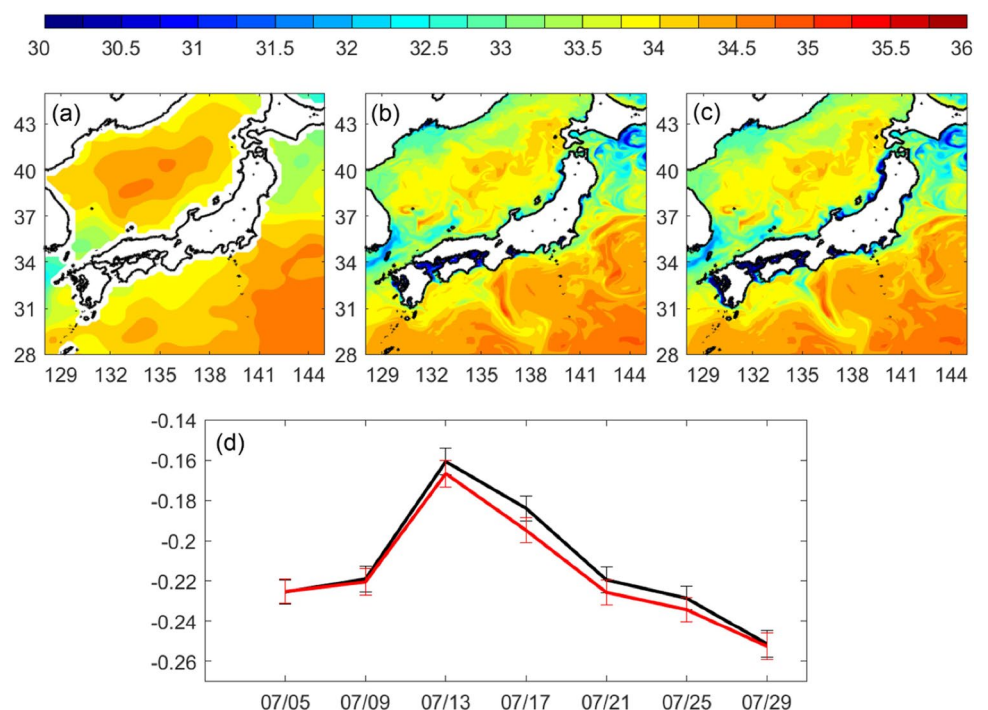


Fig. 4 Time series of salinity at **a** Ise Bay, **b** Kojima, and **c** Nagahama in the Ariake Sea. Salinity measurement observations are shown in green, Exp. Clim in black, and Exp. CamaF in red. Numbers shown in the bottom-right are the root-mean-squared error compared to observation

(Fig. 4b, c). A recent observation recorded in the eastern Pacific during a rainy period showed a salinity drop of 2–3 near the sea surface at 0.02 and 1 m depths (Clayson et al. 2019), with a rate of ~ 20 mm per hour. In the July 2020 event, the precipitation was 10–60 mm per hour near the Ariake Sea, and the salinity decreased by 2 in Exp. Clim and 5 in Exp. CamaF, but was more than 15 in the observations. The observed salinity at these two stations even dropped to nearly zero on 12 July, suggesting the buoys were directly affected by the heavy rainfall that greatly reduced the salinity values. The modeled salinity, even in the layer nearest to the surface, was below the surface by some distance (mean and standard deviation depth of 0.72 ± 0.14 m), and therefore had a limitation in representing the real surface salinity. Exp. CamaF captured the general salinity variation trend of the observations, and showed a smaller RMSE than Exp. Clim. The salinity improvement from Exp. Clim to Exp. CamaF was significant at both stations in Ariake bay ($p < 0.01$). Although the real-time river discharge used in Exp. CamaF improved the salinity, it still had a RMSE of 4–10.

The comparison between ship observations and model simulations is shown in Fig. 5. Exp. CamaF showed a significantly lower RMSE ($p < 0.01$) than Exp. Clim at the nearshore stations in Tosa Bay (Fig. 5a, b). Salinity in offshore Japan showed an insignificant difference between the two experiments (Fig. 5c, d, $p > 0.1$). A slight improvement was found in Exp. CamaF compared to Exp. Clim.

Although the modeled salinity values did not match exactly with the observations, the real-time river discharge

did indeed improve the modeled salinity near the coast. The modeled salinity did not show the apparent difference at the offshore observed stations (Fig. 5c, d). However, the difference did appear in other regions further offshore. Figure 6 shows the salinity and surface current speed differences between the two experiments. Before the heavy rain started, a small salinity difference was observed near the coast (Fig. 6a). After a week of continuous rainfall, the heavy rain regions in the south and west of Japan showed a clear freshening. Eddies and filaments of fresher water extended out from the Kii Channel (east of Shikoku) to about 300 km offshore (Fig. 6b). The salinity difference further diffused offshore with time, eventually forming a large circular oval patch of lower salinity surface water 400 km offshore (Fig. 6c). A large region of complex eddy-like salinity differences appeared east of northern Japan where mesoscale eddies were often observed within or north of the Kuroshio Extension (Chelton et al. 2011). Saltier water was also observed in coastal Japan (Fig. 6c), because the river discharge in the monthly climatology could sometimes be overestimated (i.e., 17–22 July, Fig. 2).

Comparing to the ocean currents in the southern region, the fresher circular water area was located inside the Kuroshio large meander (Fig. 6d–f). The fresher water was entrained into the Kuroshio and brought offshore with the large meander and later returned to the nearshore by the currents. Low salinity water had occasionally been observed on the surface of the Kuroshio and was suggested to originate from south and west of Japan (Imasato and

Fig. 5 Salinity at **a, b** Tosa bay and **c, d** offshore to the south of southwestern Japan. Salinities were measured at depths of **a** 0 m, **b** 10 m, **c** 1 m, and **d** 3 m. Observations are shown with solid green circles, Exp. Clim with open black circles, and Exp. CamaF with open red circles. Numbers shown in the bottom-right are the root-mean-squared error compared to observations

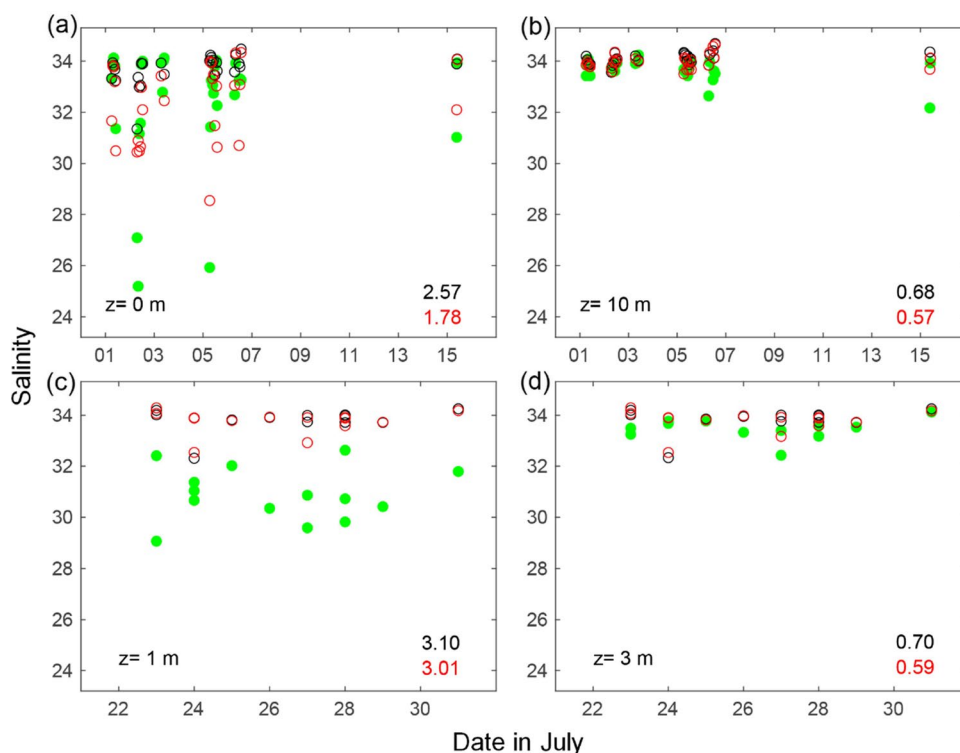
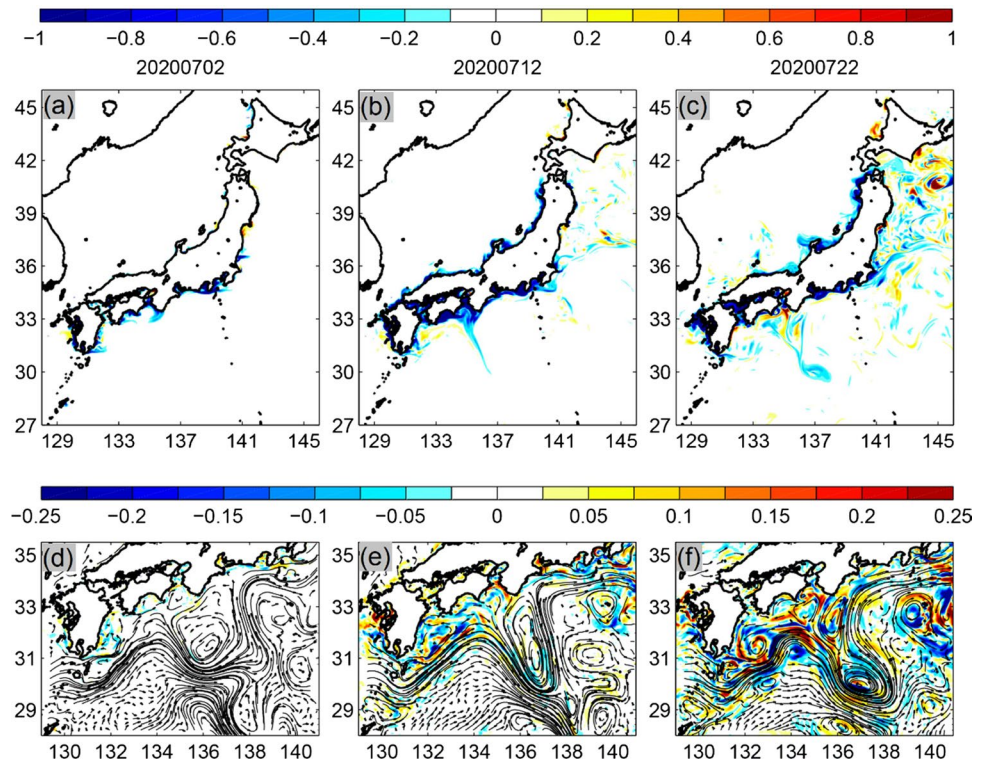


Fig. 6 Surface salinity difference **a–c** and current speed difference **d–f** between Exp. Clim and Exp. CamaF on **a, d** 2 July, **b, e** 12 July, and **c, f** 22 July. The superimposed trajectories in (d–f) are surface currents for Exp. CamaF



Qiu 1987). The freshwater discharge not only changed the salinity, but also influenced the currents (Fig. 6d–f). The currents were modified from the nearshore region to a few hundred kilometers offshore. The surface speed difference from Exp. Clim could exceed 0.2 m/s. The currents in the center of the Kuroshio large meander were weakened, and currents in the outer edge of the Kuroshio were strengthened (Fig. 6f). The absolute vorticity changes from Exp. Clim to Exp. CamaF in the Kuroshio large meander region (135.5–139°E, 28.8–31.5°N) were reduced by $-3.38 \times 10^{-7} \text{ s}^{-1}$. The trapping ability

of rotating fluid is determined by the rotation versus the translation speed (Flierl 1981), and the reduction of vorticity in Exp. CamaF suggested the amount of water parcels trapped in the Kuroshio large meander area may be reduced.

The passive particle tracking experiments were conducted to examine the cross-shelf exchange in the heavy rain region near Shikoku. The number of particles in each zone depended on the size of each defined area. The percentage of particles of each defined area (Table 1) was calculated by the number of particles in each domain divided by the

Table 1 Particle distribution (%) present in each zone after being released and tracked at depths of 5 m and 50 m on the initial and final days, based on hourly and daily background currents. Zones 1 and 4 were located on the shelf surrounding Shikoku Island, zones 5–7

were off the shelf in the south of Japan (Fig. 8). The percentages are the number of particles in each zone divided by the total released particles

Zone	Initial	Final: hourly data				Final: daily data			
		Exp. Clim		Exp. CamaF		Exp. Clim		Exp. CamaF	
		5 m	50 m	5 m	50 m	5 m	50 m	5 m	50 m
1	19.20	23.03	14.38	22.33	14.28	22.66	15.80	15.18	16.32
2	17.61	5.81	5.38	5.87	5.38	3.97	8.83	4.99	8.65
3	14.41	4.93	6.98	6.61	7.77	3.43	7.80	2.66	6.90
4	48.77	47.28	55.43	46.51	55.42	46.17	53.60	49.65	53.91
5	–	0.44	1.64	0.66	1.58	0.05	1.07	4.51	1.08
6	–	12.69	15.57	11.73	14.90	23.24	12.89	22.53	13.15
7	–	5.82	0.63	6.28	0.68	0.49	–	0.47	–

number of total particles released in all areas. Particles that departed at a depth of 5 m mostly stayed on the shelf (> 70%, Table 1). There were 18–19% of particles that went offshore, with part of them becoming trapped in the Kuroshio, others were transported downstream into the Kuroshio Extension to the east of Japan, and some of the particles were transported southward to the east of Kyushu (Fig. 7). Particle distributions were different between the two experiments (Fig. 7). Particles arrived east of Kyushu earlier and in larger numbers in Exp. CamaF than in Exp. Clim (Fig. 7, Table 1). Particles observed in the Kuroshio meander (zone 6, Table 1) were reduced in Exp. CamaF (11.73%) compared to Exp. Clim (12.69%). Fewer particles being trapped in the Kuroshio meander could be caused by the weakening of Kuroshio vorticity. The Kuroshio extension region appeared to have more particles in Exp. CamaF than in Exp. Clim (Fig. 7 and Table 1), especially for those that originated from Tosa Bay (zone 2). The particles redistribution on the shelf also varied between experiments. At the end of the simulation, particles in Bungo Channel (zone 1) showed a greater percentage in

Exp. Clim than in Exp. CamaF. Particles in Tosa Bay (zone 2) and Kii Channel (zone 3) were reduced significantly from the initial date, with the reduction being less in Exp. CamaF than in Exp. Clim. The amount of particles that remained in the Seto Inland Sea was similar (> 45%) among the experiments, in which Exp. CamaF showed a slightly lower percentage of particles than Exp. Clim.

The connectivity matrix showed the detailed redistribution of particles between the different sub-domains (Table 2). In Exp. Clim, particles released in Bungo Channel (zone 1) mostly stayed in that zone (84.01%), a small percent of particles were transported eastward and northward to Tosa Bay (zone 2) and Seto Inland Sea (zone 4), and some went off-shelf or entered Kuroshio (zones 5, 6, 7). Zone 1 released particles in Exp. CamaF had slightly less retention (83.19%) in the same zone. Instead, more particles were transported off-shelf to the east of Kyushu (zone 5) and into the Kuroshio meander region (zone 6), which could also be seen in Fig. 7 (green dots).

Fig. 7 Passive particles released in the heavy rain region surrounding Shikoku at a depth of 5 m and their distributions on **a, d** 11 July, **b, e** 21 July, and **c, f** the final date on 31 July for **a–c** Exp. Clim, and **d–f** Exp. CamaF. Color represents different release regions: Bungo Channel (zone 1, green), Tosa Bay (zone 2, blue), Kii Channel (zone 3, red), and Seto Inland Sea (zone 4, magenta) as shown in Fig. 1c

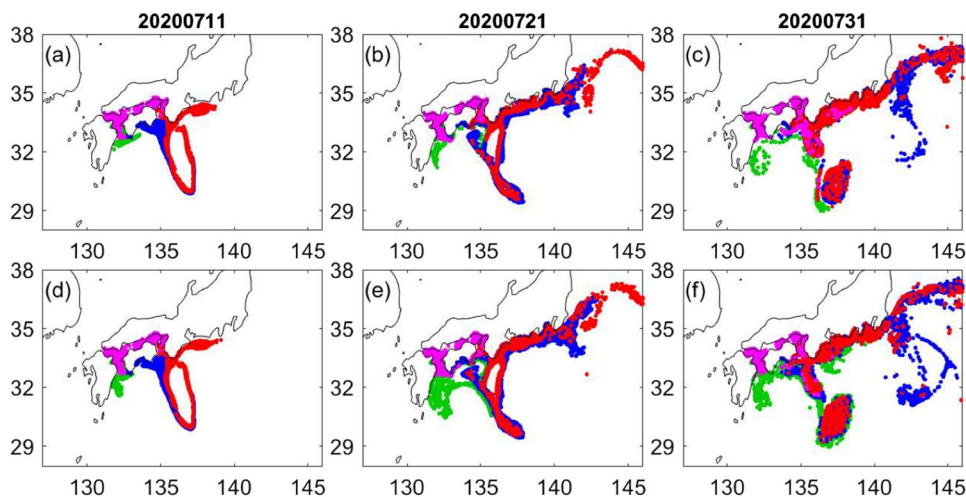


Table 2 Connectivity matrix showing the percentages of particles that moved from one zone to another after being released and tracked at a depth of 5 m. The zone definitions are the same as Table 1 and

Exp. Clim	start end	1	2	3	4	5	6	7
	1	84.01	4.30	–	4.79	1.95	4.72	0.24
	2	0.07	30.98	0.32	0.05	0.07	47.52	21.00
	3	–	–	35.49	19.53	–	27.67	17.32
	4	13.33	0.05	0.11	86.03	0.03	0.46	–
Exp. CamaF	1	83.19	2.03	0.16	5.23	2.89	6.45	0.05
	2	0.18	33.28	0.22	–	0.03	42.40	23.88
	3	–	0.01	46.76	12.75	–	23.84	16.64
	4	12.62	0.06	0.23	86.95	0.04	0.09	–

Fig. 8 Percentages are the number of particles in each destination zone divided by the number of particles released in each departure zone. The sum of each row is about 100 (%)

Particles released in Tosa Bay (zone 2) had a small percentage (< 35%) remaining in the same area, and more than 60% of those particles were taken offshore into the Kuroshio (Table 2). Exp. Clim had less retention (30.98%) in the released area than Exp. CamaF (33.28%), yet more particles were observed in the Kuroshio extension region (zone 7) in Exp. CamaF (23.88%) than Exp. Clim (21%) (Fig. 7 and Table 2). Less than half of the particles from Kii Channel (zone 3) remained there, others released there became the major group that arrived in the Kuroshio (zone 6) and in the Kuroshio Extension (zone 7), and some reached the Seto Inland Sea (zone 4). Exp. Clim had less local retention for the particles that departed from Kii Channel, and more particles moved to the Seto Inland Sea and the Kuroshio compared to Exp. CamaF (Table 2 and Fig. 7). Greater than 85% of the particles released in the Seto Inland Sea (zone 4) remained in the same region. Only about 13% of particles were transported southwest to zone 1, less than 1% arrived at other zones, and none of the particles reached the Kuroshio Extension in zone 7. Exp. CamaF had greater retention in zone 4 and less particles went offshore to zones 5–7 in comparison to Exp. Clim (Table 2 and Fig. 7).

Particles were also released and tracked in sub-surface water (50 m) at the same horizontal locations in the seas around Shikoku Island to examine the subsurface current variation from Exp. Clim to Exp. CamaF. Although the freshwater discharge was mainly distributed near the surface, the particle distribution map also showed some different particle distributions in the subsurface water between Exp. Clim and Exp. CamaF (Fig. 8). Particles in the subsurface layer tended to be transported along the edge of the Kuroshio without entering its center (Fig. 8). Calculating the arrival rate quantitatively, around 17% of particles went offshore to zones 5, 6, and 7 (Table 1). Particles in different

zones showed a different percentage of retention between the two experiments, suggesting the subsurface water also changed with the input of real-time river discharge. The subsurface particles showed a similar variation to the near surface particles, i.e., particles in zone 1 were more in Exp. CamaF than Exp. Clim, and particles in zone 3 showed the opposite tendency, but the differences between the two experiments were smaller in the subsurface than near surface layer.

The two particle tracking experiments (Exp. Clim and Exp. CamaF) described above suggest that the enhanced river discharges during the heavy rain period changed the shelf circulation patterns in the coastal regions. Looking into the daily volume transport at Bungo Channel and Kii Channel, the water exchange in the Seto Inland Sea via the two channels seemed to be strengthened in Exp. CamaF in comparison to Exp. Clim (Fig. 9), although the difference was not significant ($p \sim 0.6$). The Bungo Channel and the Kii Channel are the two major gates connecting the Seto Inland Sea to the open ocean. The surface-to-bottom integrated transport at the two channels showed the inflow from Kii Channel and the outflow from Bungo Channel were both stronger in Exp. CamaF than in Exp. Clim during the heavy rain period in early July (Fig. 9a), indicating a stronger water exchange between shelf seas and the open ocean. The enhanced water exchange was also observed in the two channels individually (Fig. 9b, c). In the Kii Channel, Exp. CamaF showed a significantly ($p \sim 0.05$) stronger inflow near the surface and outflow in the subsurface than Exp. Clim in early July. The tendency in Bungo Channel reversed, although the difference in the subsurface was not very clear and insignificant ($p \sim 0.7$). Note that the in-and-out transport summation of the two channels was not zero values, because of the existence of an additional smaller

Fig. 8 Same as Fig. 7, but for particles released and tracked at a depth of 50 m

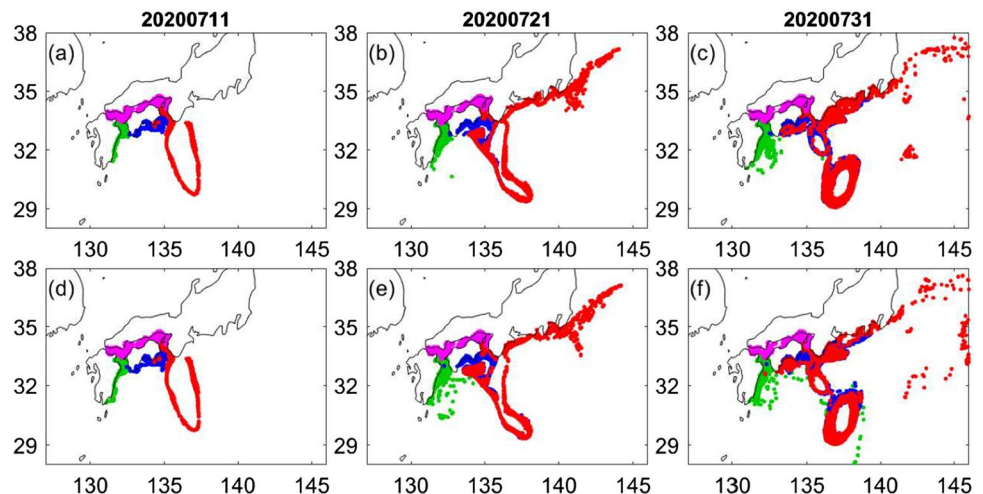
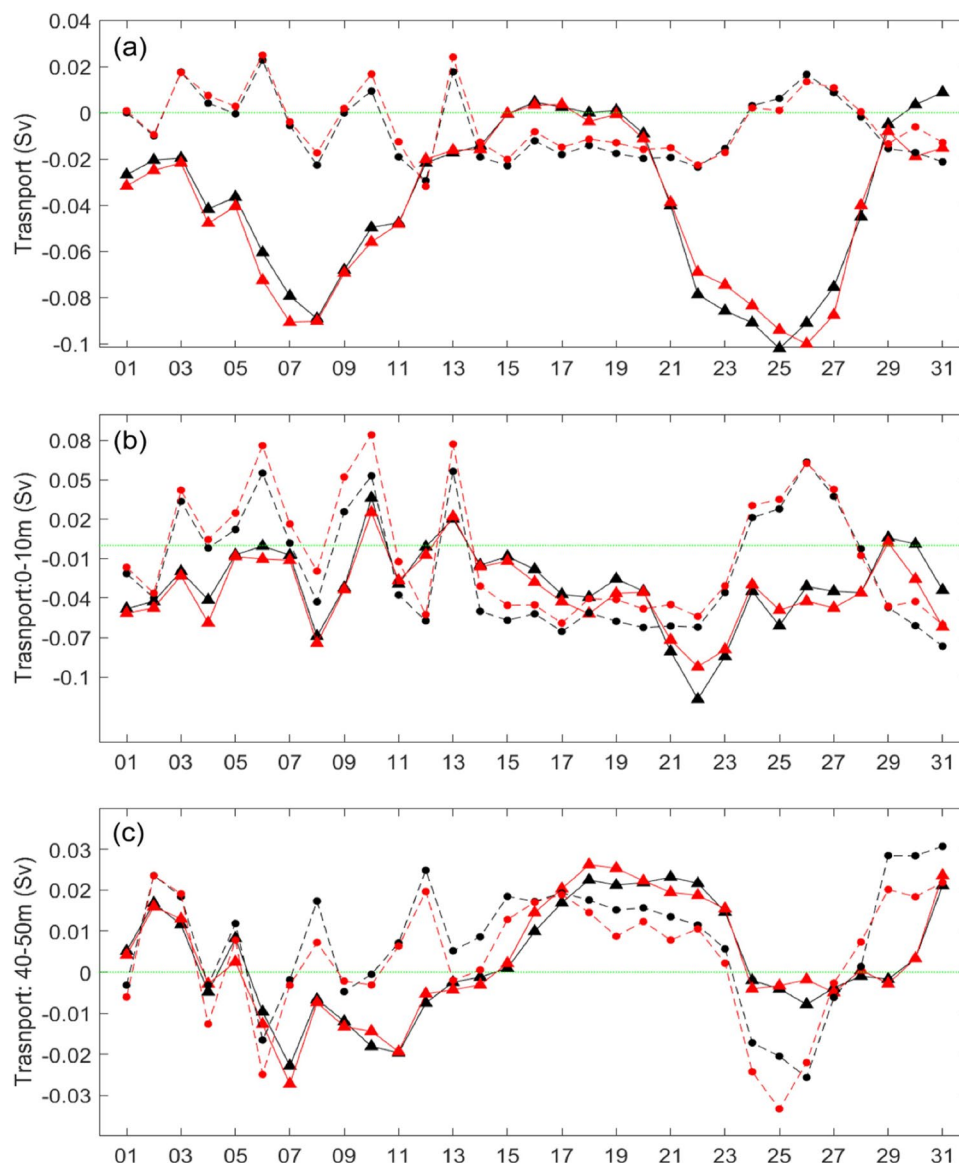


Fig. 9 Quantification of the changes in volume transport between Exp. Clim and CamaF. Daily mean transport at the Bungo Channel (solid lines with triangles) and the Kii Channel (dashed line with circles) for Exp. Clim (black) and Exp. CamaF (red) for **a** surface to bottom integration **b** 0–10 m integration, and **c** 40–50 m integration in July 2020. Unit = Sv = $10^6 \text{ m}^3/\text{s}$, positive represents northward transport moving into the channel, southward transport flows out of the channel

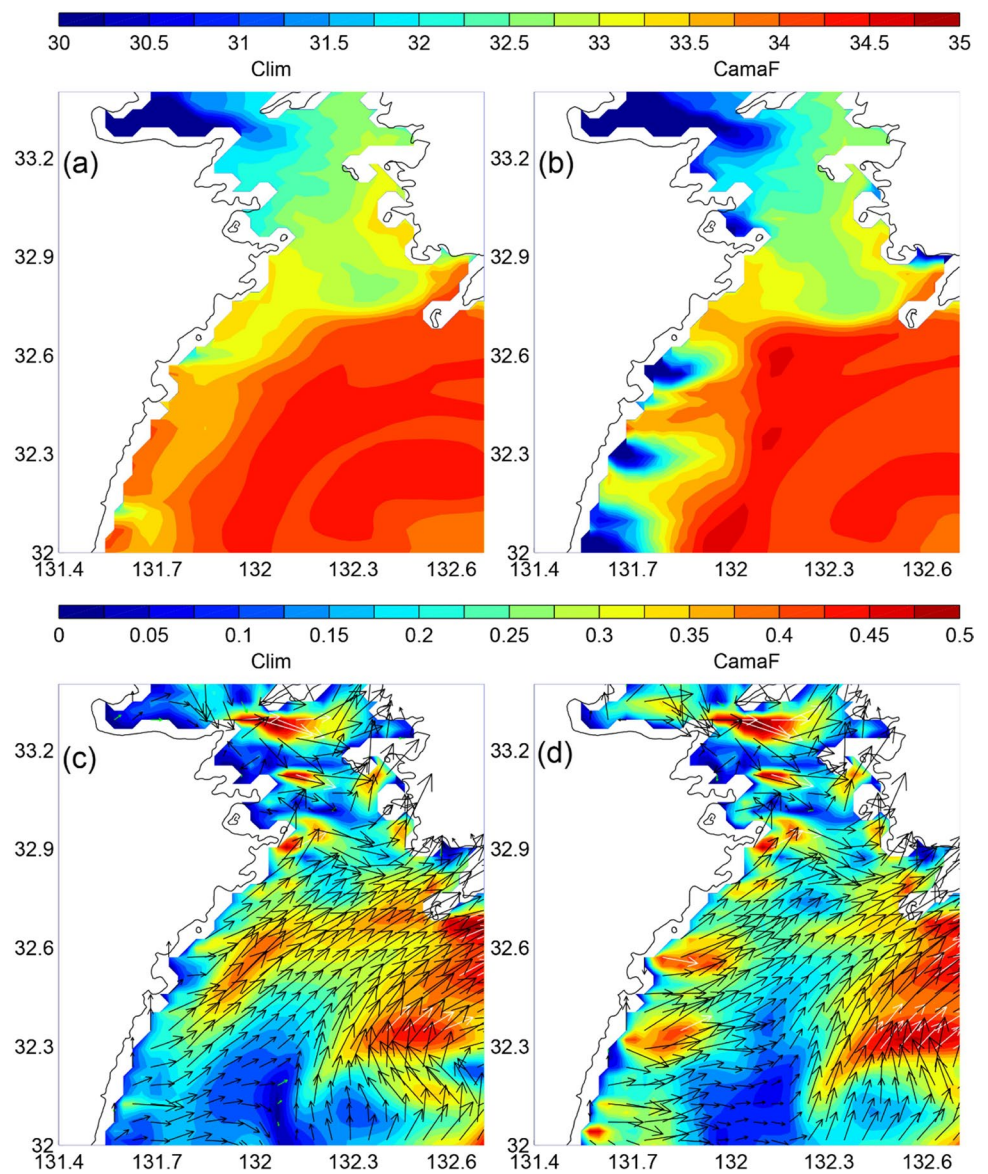


channel opening (Kanmon Strait) in the northwestern Seto Inland Sea that connects to the Sea of Japan.

Differences in the channel or bay circulation between the two experiments could be seen in the current fields with the change of salinity (Figs. 10, 11, and 12, Sup. A1–3). In Bungo Channel (zone 1), the large river discharge during the first peak of heavy rain in early July induced a clear low salinity plume in the western Bungo Channel in Exp. CamaF (Fig. 10b, Sup. A1), which was not seen in the Exp. Clim (Fig. 10a). The low salinity plume induced the local jets, which modified the currents in the western Channel in Exp. CamaF in comparison to Exp. Clim (Fig. 10c, d). A similar feature was also seen in Tosa Bay (Fig. 11, Sup. A2). The low salinity plumes appeared in the western Tosa Bay (Fig. 11b, Sup. A2), where a local jet was observed

(Fig. 11d, Sup. A2). The large low salinity region shown in the center of the Bay also appeared as a local strengthening current along the edge of the low salinity plume where the salinity gradient was strong (Fig. 11b, d). In Kii Channel, low salinity water flowed along the western and eastern channels, and a few small plumes appeared outside of the western Channel in Exp. CamaF (Fig. 12, Sup. A3). The isohalines were tilted across the Kii Channel, which showed different types of the buoyant plume in the west and east of the channel (Figs. 13 and 14). Basically, the contrast between the west and east sides of the channel was caused by the advection of the strong ambient currents (Fig. 12c, d). Two different types of plumes, a bottom-advected plume and a surface-advected plume (Yankovsky and Chapman 1997) were seen in the Kii Channel. In the inner part of the western

Fig. 10 Daily mean surface salinity and surface currents at the Bungo Channel (zone 1) on 6 July. **a, c:** Exp.Clim and **b, d:** Exp.CamaF. Color shading in **c, d** represents the current speed (m/s). Vectors in different colors show the speeds in different ranges for better visualization: <0.05 m/s (green), 0.05–0.4 m/s (black), >0.4 m/s (white)



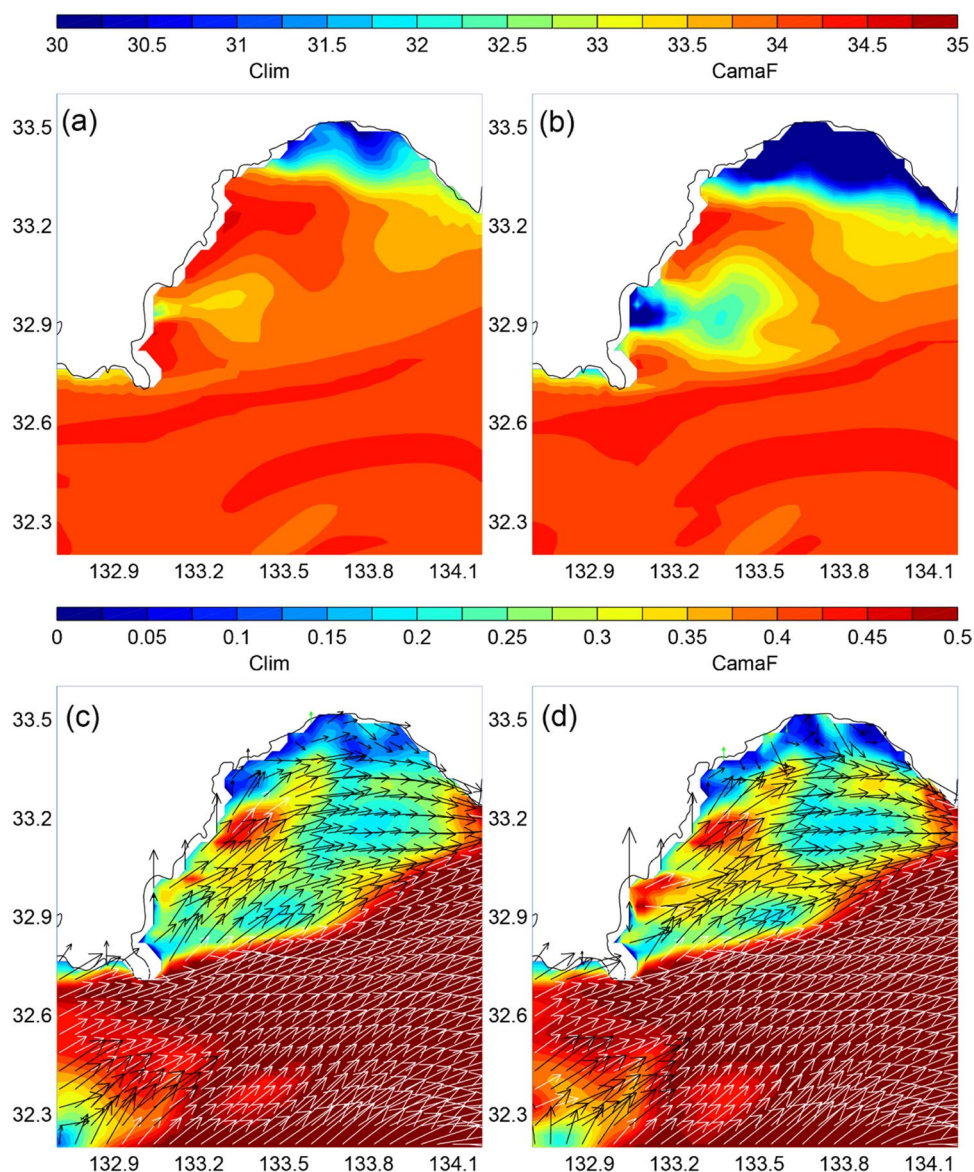
channel, the isohaline crossed the bottom and was parallel to the coast, which was characterized as the bottom-advected plume (Fig. 13c, d). More fresh water in Exp. CamaF deepened the isohaline, and strengthened the bottom-advected plume on 10 July. In the eastern Channel, the isohalines distribution were mostly parallel to the depth, which was considered to be a surface-advected plume (Fig. 13e, f). The heavy rain resulted in fresher water appearing near the surface, and strengthened the surface-advected plume in Exp. CamaF in comparison to Exp. Clim on 10 July (Fig. 13e, f). As the rain continued and accumulated for a few more days, the tilted isohalines across the channel further deepened on the western channel (Fig. 14a, b). In the western channel, the plume had mostly changed into being surface-advected, Exp. CamaF showed a stronger stratification than Exp. Clim

(Fig. 14c, d), and the fresher water was further advected offshore. In the eastern channel, the plume remained surface-advected, with a stronger plume shown in Exp. CamaF than in Exp. Clim (Fig. 14e, f).

8 Conclusion and discussion

The present study explored the influence of changes in river discharge on the variation of coastal salinity and currents based on ocean model simulations. The experiment with real-time river discharge (Exp. CamaF) showed a lower RMSE and better fit to observation compared to the case with monthly climatology rivers (Exp. Clim).

Fig. 11 Same as Fig. 10, but for Tosa Bay (zone 2)

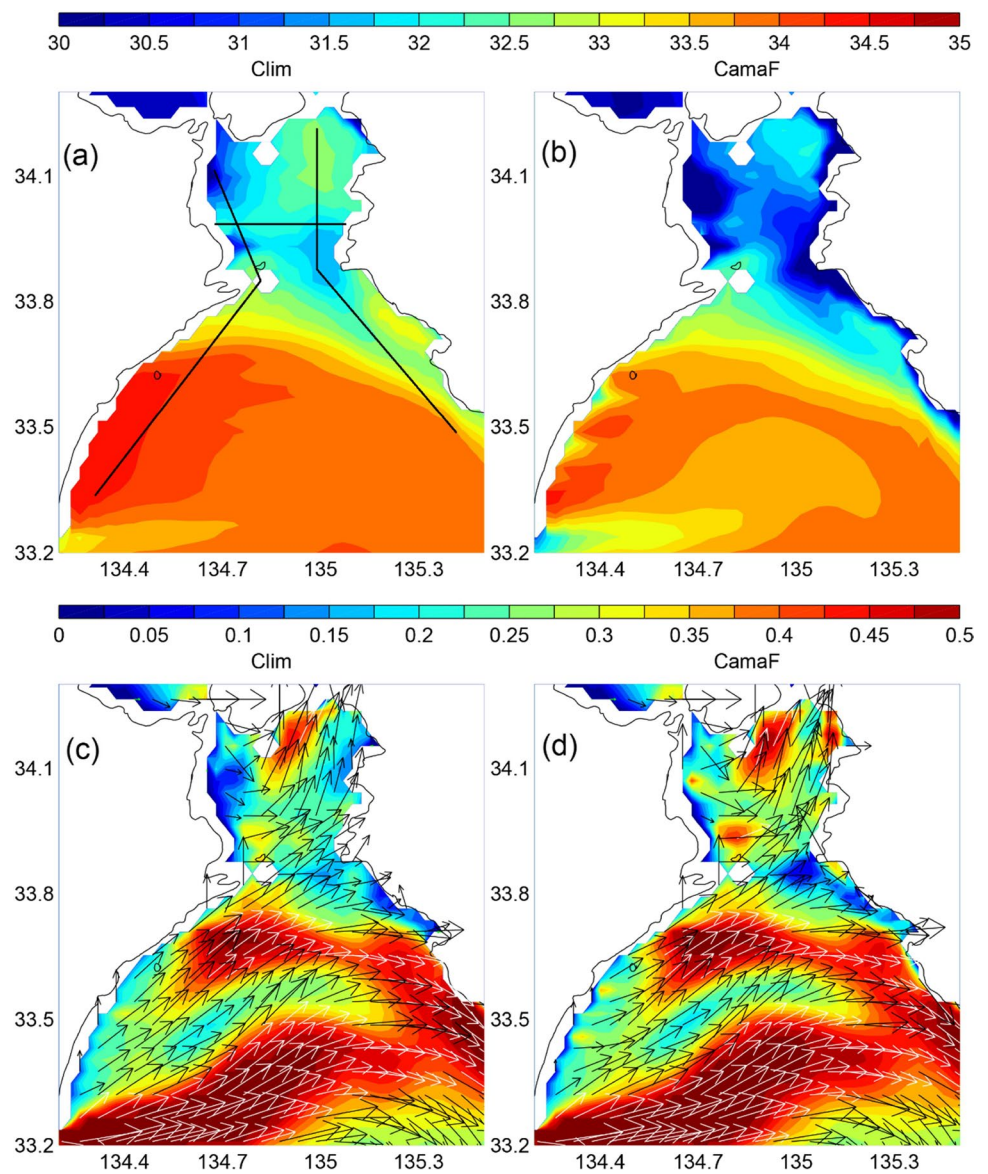


The real-time river discharge (Exp. CamaF) led to distinct freshening in the heavy rain region of southwestern Japan. The heavy rain not only influenced the nearshore area, but the freshwater also went out of the coastal areas and entered the Kuroshio in some areas and arrived hundreds of kilometers offshore. The fresher water modified the Kuroshio speed, weakened the relevant vorticity owing to the additional buoyancy inputs from the nearshore side against the ambient buoyancy condition in the offshore side associated with the Kuroshio, and the weakening of the vorticity resulted in less trapping of particles inside the Kuroshio meander jet.

The fresher water modified the coastal currents, resulting in different coastal circulation and shelf exchange shown in the passive particle tracking and the

flow field. The resulting change in the near-shore circulations caused by input of the real-time river discharge suggests that the extreme freshwater input did not simply lead to strengthening circulation or enhanced water mass exchange between the shelf and offshore regions. For example, our simulations demonstrated more retention of the particles in some shelf regions in Exp. CamaF than in Exp. Clim (Table 2). The effects of the extreme river discharges on the coastal circulations were also affected by the local topography around the river mouths and the coastal regions, the ambient density/geostrophic current structures, and the other external forcing factors such as local wind and precipitation. Further development of ocean modeling would be required for elucidating more detailed views of the underlying mechanisms. In the

Fig. 12 The same as Fig. 10, but for Kii Channel (zone 3). The sections shown in **a** were used for showing vertical profiles in Figs. 13 and 14

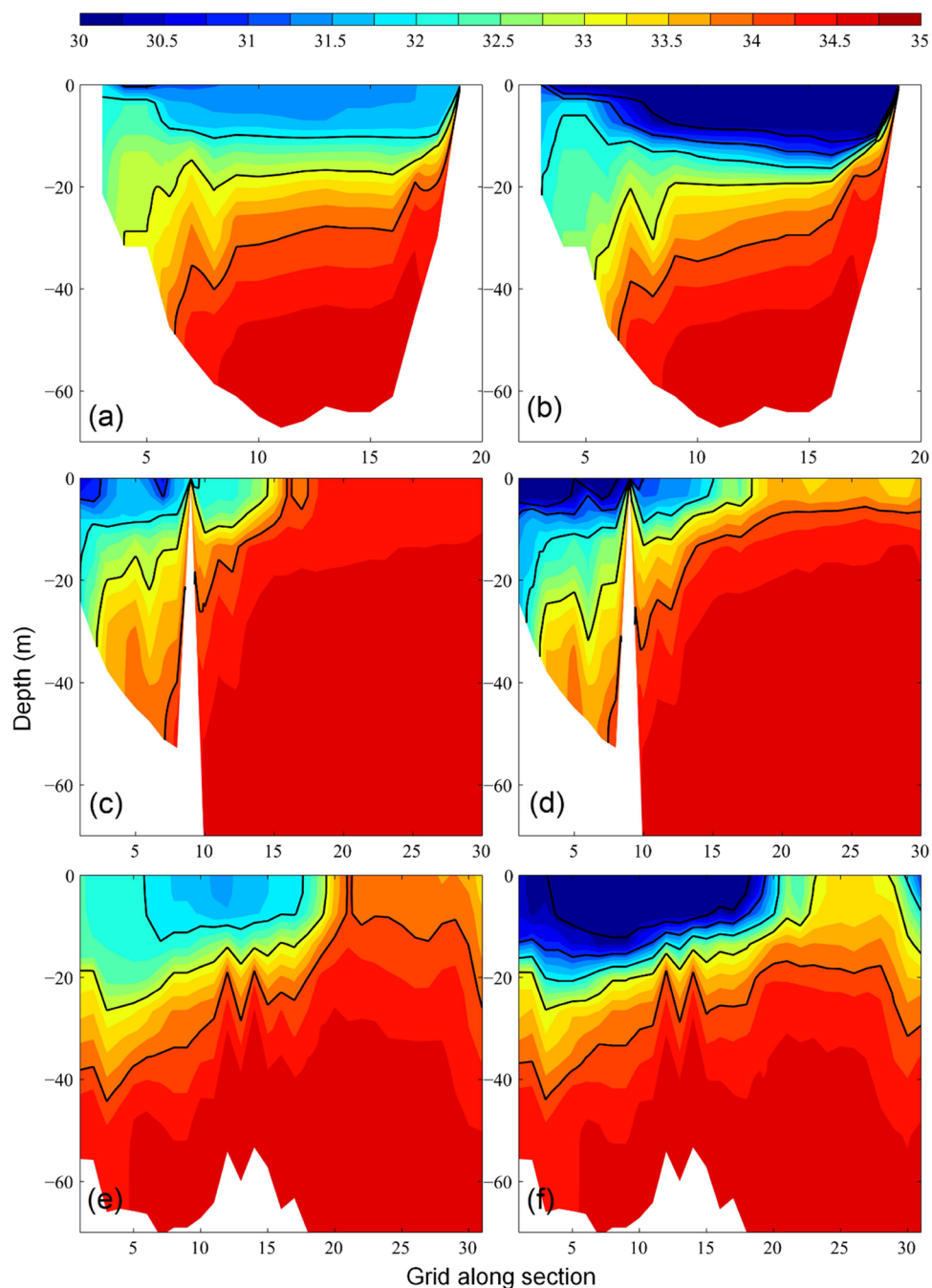


1-month integration, the particle distribution difference among the study regions between Exp. Clim and Exp. CamaF was close to significant ($p \sim 0.2$). The difference would likely grow with longer integration because the river discharge differed not only during heavy rain periods, but also on general days. Worth noticing is that the transport difference was also observed during the dry period in the 1-month simulation, indicating the real-time discharge was not limited to its influence in the heavy rain period.

The ability to simulate salinity in the near-surface water compared to observations was improved with the input of real-time river discharge. However, the errors remained nonnegligible, especially at the sea surface. JCOPE-T DA applied terrain-following vertical

coordinates in the near-surface layers, and its first layer was below the sea surface. In such a case, the model had limitations in simulating the exact surface salinity. During the extraordinary precipitation when buoy stations may even observe the nearly zero salinity due to the continuous heavy rainfall and the direct rainfall over the sea surface, the model would have difficulty in reproducing such a salinity reduction. In addition to rainwater coming from rivers, there was also the rain that directly fell onto the sea, as well as the freshwater input directly from the coast without a river mouth that both led to biases of model simulation. In this study, the experiments were run freely without data assimilation for isolating the effect of river discharge. In the operational hindcast of the forecast system, the surface salt

Fig. 13 Isohaline **a, b** across, **c, d** along the west side, and **e, f** along the east side of the Kii Channel on 10 July for (left) Exp. Clim and (right) Exp. CamaF. The sections were marked in Fig. 12a

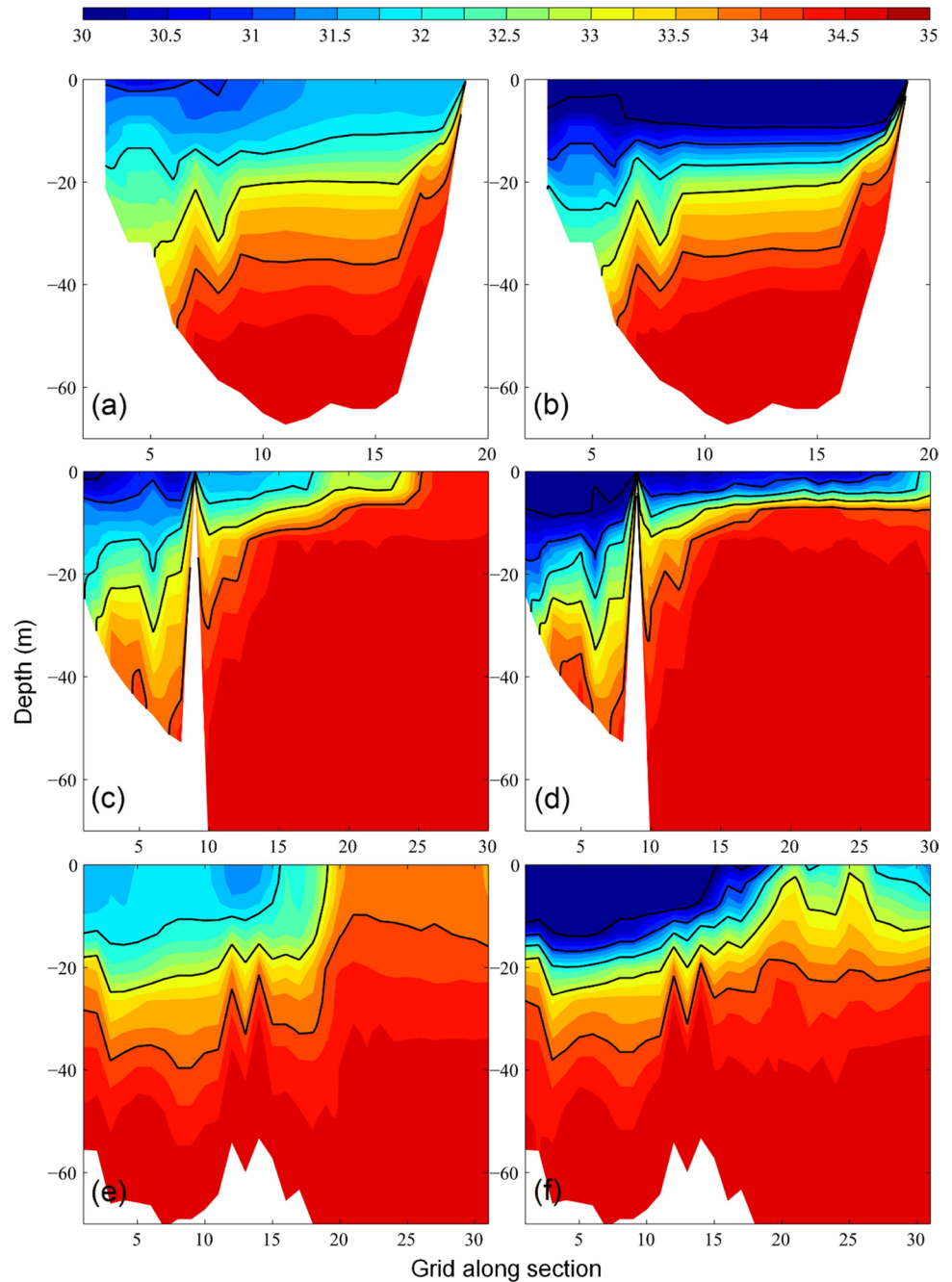


flux was assimilated into the model that could improve the salinity bias.

Particles released in the Seto Inland Sea (zone 4) showed the least offshore movement of particles in near-surface and subsurface waters. The large percentage of particles that stayed in the Seto Inland Sea zone 4 could be caused by its inland topography. The tidal effect was considered to affect the shelf seawater exchange (Lin et al. 2020), which could alter the retention of particles inside the Seto Inland Sea.

To examine the sensitivity on the time interval of data, we repeated the particle tracking using the daily averaged ocean currents. The daily particle distributions were rather different from the hourly tracking (Figs. 13 and 7). The current field was different from hourly output, much less particles in the daily experiment arrived at the Kuroshio extension region (Fig. 15) during the same integration period. Not only the distribution was changed, but an increase or decrease in percentage of particles occurred from Exp. Clim to Exp. CamaF could also be different in

Fig. 14 Same as Fig. 13, but for 14 July



some areas, i.e., zones 3, 4, and 7 at depth of 5 m, and zones 1, 3, and 6 at a depth of 50 m (Table 1). The daily averaged data filtered out large percentage of the tidal signal, which may be the main reason responsible for the difference. A previous study suggested the exclusion of the tidal effect could accelerate the shelf exchange (Lin et al. 2020). The enhancement of shelf exchange could also be seen in the daily experiments, which show a greater percentage of particles moving offshore near the surface compared to in the hourly experiments (Table 1). Although

the daily output remains as the primary option for most of the reanalysis dataset owing to its benefit in saving storage space, its missing information and therefore potential bias in interpretation should be noted.

The real-time river discharge improved the coastal salinity during the selected heavy rain period. To confirm the change from Exp. Clim to Exp. CamaF is robust but not random, the additional ensemble experiments were conducted by perturbing the initial condition of Exp. CamaF. The ensemble runs and Exp. CamaF both showed

Fig. 15 Same as Fig. 7 for the particles released and tracked at depth of 5 m, but based on daily current fields

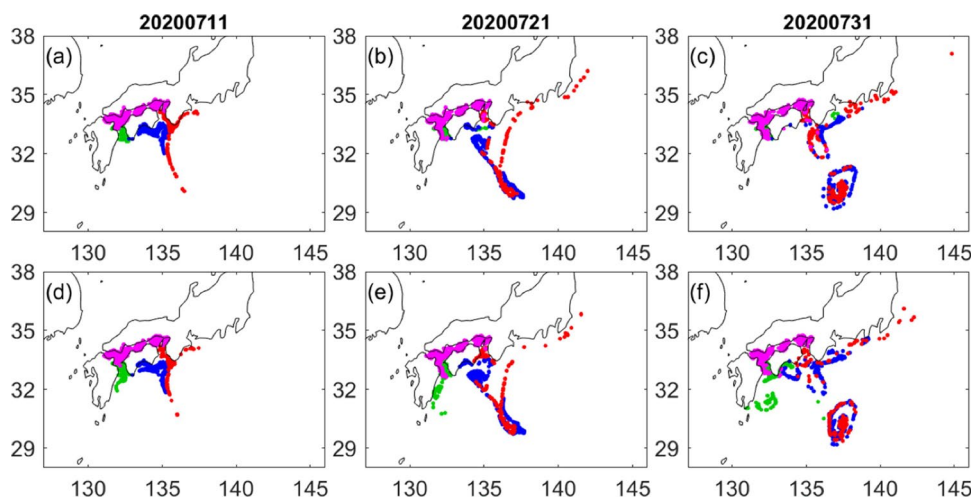
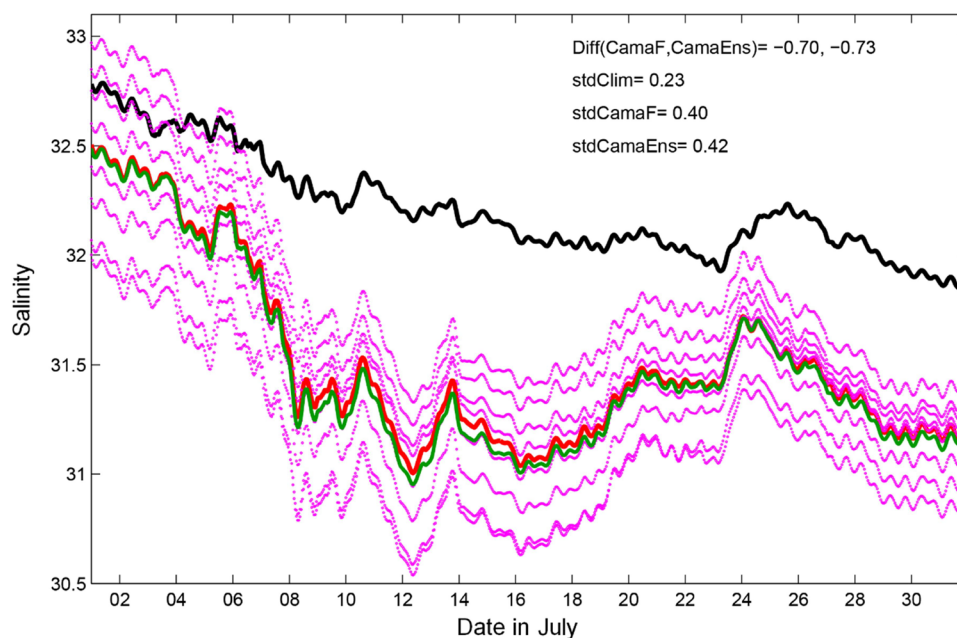


Fig. 16 The shelf (depth ≤ 200 m) averaged salinity in July 2020 around Japan for Exp. Clim (black), Exp. CamaF (red), and the ensemble runs (magenta) and mean (green) by perturbing the initial condition of Exp. CamaF



smaller standard deviations than their differences with Exp. Clim, indicating the differences between Exp. Clim and Exp. CamaF were robust (Fig. 16). We also noticed that the ensemble spread gradually reduced with time, suggesting the results converged. Besides, we repeated the comparison against the observations described earlier (Figs. 4 and 5). The ensemble runs shown the similar results as Exp. CamaF, the difference between ensemble runs and Exp. Clim were significant at Ise Bay and Ariake Sea ($p < 0.01$, i.e., Fig. 4), and was nearly significant at Tosa Bay ($p = 0.2$, i.e., Fig. 5a), but was insignificant in the offshore region ($p > 0.5$, i.e., Fig. 5c). Whether the improvement remains for a normal or dry season is the next step for examination. The real-time river discharge

is now planned to replace the default monthly climatology rivers for JCOPE-T DA for better simulating the coastal salinity and currents, especially during extreme conditions.

Supplementary Information The online version contains supplementary material available at <https://doi.org/10.1007/s10236-023-01551-1>.

Acknowledgements X. Guo thanks the support of a Grant-in-Aid for Scientific Research (MEXT KAKENHI, grant number: 22H05206). Research product of Today's Earth that was used in this paper was supplied by Japan Aerospace Exploration Agency and Institute of Industrial Science, The University of Tokyo.

Data availability The datasets generated during and/or analyzed during the current study are available from the corresponding author on reasonable request.

Declarations

Conflict of interest The authors declare no competing interests.

Open Access This article is licensed under a Creative Commons Attribution 4.0 International License, which permits use, sharing, adaptation, distribution and reproduction in any medium or format, as long as you give appropriate credit to the original author(s) and the source, provide a link to the Creative Commons licence, and indicate if changes were made. The images or other third party material in this article are included in the article's Creative Commons licence, unless indicated otherwise in a credit line to the material. If material is not included in the article's Creative Commons licence and your intended use is not permitted by statutory regulation or exceeds the permitted use, you will need to obtain permission directly from the copyright holder. To view a copy of this licence, visit <http://creativecommons.org/licenses/by/4.0/>.

References

- Blumberg AF, Mellor GL (1987) A description of a three-dimensional coastal ocean circulation model. Three-Dimensional Coastal Ocean Models, vol. 4, N. Heaps, Ed., American Geophysical Union pp 208
- Carniel S, Warner JC, Chiggiato J, Sclavo M (2009) Investigating the impact of surface wave breaking on modeling the trajectories of drifters in the northern Adriatic Sea during a wind-storm event. *Ocean Model* 30(2):225–239
- Chassignet E et al (2009) US GODAE: global ocean prediction with the HYbrid coordinate ocean model (HYCOM). *Oceanogr* 22(2):64–75
- Chelton DB, Schlax MG, Samelson RM (2011) Global observations of nonlinear mesoscale eddies. *Prog Oceanogr* 91(2):167–216
- Clayson CA, Edson JB, Paget A, Graham R, Greenwood B (2019) Effects of rainfall on the atmosphere and the ocean during spuRS-2. *Oceanogr* 32(2):86–97
- Dai A, Qian T, Trenberth KE, Milliman JD (2009) Changes in continental freshwater discharge from 1948 to 2004. *J Clim* 22(10):2773–2792
- Egbert GD, Erofeeva SY (2002) Efficient inverse modeling of barotropic ocean tides. *J Atmos Oceanic Tech* 19(2):183–204
- Flierl GR (1981) Particle motions in large-amplitude wave fields. *Geophys Astrophys Fluid Dyn* 18:39–74
- Garvine RW (1987) Estuary plumes and fronts in shelf waters: a layer model. *J Phys Oceanogr* 17(11):1877–1896
- Geyer WR, MacCready P (2014) The estuarine circulation. *Annu Rev Fluid Mech* 46(1):175–197
- Heki K, Arief S (2022) Crustal response to heavy rains in Southwest Japan 2017–2020. *Earth Planet Sci Lett* 578:117325
- Horner-Devine AR, Hetland RD, MacDonald DG (2015) Mixing and transport in coastal river plumes. *Annu Rev Fluid Mech* 47(1):569–594
- Imasato N, Qiu B (1987) An event in water exchange between continental shelf and the Kuroshio off Southern Japan: Lagrangian tracking of a low-salinity water mass on the Kuroshio. *J Phys Oceanogr* 17(7):953–968
- Kawase H, Imada Y, Tsuguti H, Nakaegawa T, Seino N, Murata A, Takayabu I (2020) The heavy rain event of July 2018 in Japan enhanced by historical warming. *Bull Am Meteor Soc* 101(1):S109–S114
- Lin L, Liu D, Guo X, Luo C, Cheng Y (2020) Tidal effect on water export rate in the eastern shelf seas of China. *J Geophys Res: Oceans* 125:e2019JC015863
- Ma W, Ishitsuka Y, Takeshima A, Hibino K, Yamazaki D, Yamamoto K, Kachi M, Oki R, Oki T, Yoshimura K (2021) Applicability of anationwide flood forecasting system for Typhoon Hagibis 2019. *Sci Rep* 11:10213. <https://doi.org/10.1038/s41598-021-89522-8>
- Miller JR, Russell GL, Caliri G (1994) Continental-scale river flow in climate models. *J Clim* 7(6):914–928
- Miyazawa Y, Zhang R, Guo X, Tamura H, Ambe D, Lee J-S, Okuno A, Yoshinari H, Setou T, Komatsu K (2009) Water mass variability in the western North Pacific detected in a 15-year eddy resolving ocean reanalysis. *J Oceanogr* 65(6):737–756
- Miyazawa Y, Varlamov SM, Miyama T et al. (2017) Assimilation of high-resolution sea surface temperature data into an operational nowcast/forecast system around Japan using a multi-scale three-dimensional variational scheme. *Ocean Dynamics* 67:713–728. <https://doi.org/10.1007/s10236-017-1056-1>
- Miyazawa Y, Varlamov SM, Miyama T, Kurihara Y, Murakami H, Kachi M (2021) A nowcast/forecast system for Japan's coasts using daily assimilation of remote sensing and in situ data. *Remote Sens* 13(13):2431
- Morimoto A, Dong M, Kameda M, Shibakawa T, Hirai M, Takejiri K, Guo X and Takeoka H (2022) Enhanced cross-shelf exchange between the pacific ocean and the bungo channel. Japan related to a heavy rain event. *Front Mar Sci* 9:869285. <https://doi.org/10.3389/fmars.2022.869285>
- Press WH, Flannery BP, Teukolsky SA, Vetterling WT (1992) Numerical recipes in FORTRAN 77: The Art of Scientific Computing. Cambridge University Press
- Sasaki H, Kida S, Furue R, Aiki H, Komori N, Masumoto Y, Miyama T, Nonaka M, Sasai Y, Taguchi B (2020) A global eddying hindcast ocean simulation with OFES2. *Geosci Model Dev* 13(7):3319–3336
- Trenberth KE, Smith L, Qian T, Dai A, Fasullo J (2007) Estimates of the global water budget and its annual cycle using observational and model data. *J Hydrometeorol* 8(4):758–769
- Troselj J, Sayama T, Varlamov SM, Sasaki T, Racault M-F, Takara K, Miyazawa Y, Kuroki R, Yamagata T, Yamashiki Y (2017) Modeling of extreme freshwater outflow from the north-eastern Japanese river basins to western Pacific Ocean. *J Hydrol* 555:956–970
- Urakawa LS, Kurogi M, Yoshimura K, Hasumi H (2015) Modeling low salinity waters along the coast around Japan using a high-resolution river discharge dataset. *J Oceanogr* 71(6):715–739
- Varlamov SM, Guo X, Miyama T, Ichikawa K, Waseda T, Miyazawa Y (2015) M2 baroclinic tide variability modulated by the ocean circulation south of Japan. *J Geophys Res: Oceans* 120(5):3681–3710
- Yankovsky AE, Chapman DC (1997) A simple theory for the fate of buoyant coastal discharges. *J Phys Oceanogr* 27(7):1386–1401
- Yoshimura K, Sakimura T, Oki T, Kanae S, Seto S (2008) Toward flood risk prediction: a statistical approach using a 29-year riverdischarge simulation over Japan. *Hydrol Res Lett* 2:22–26
- Yamazaki D, Kanae S, Kim H, Oki T (2011) A physically based-description of floodplain inundation dynamics in a global river routingmodel. *Water Resour Res* 47:W04501. <https://doi.org/10.1029/2010WR009726>.
- Zhao N, Manda A, Guo X, Kikuchi K, Nasuno T, Nakano M, Zhang Y, Wang B (2021) A Lagrangian view of moisture transport related to the heavy rainfall of July 2020 in Japan: importance of the moistening over the subtropical regions. *Geophys Res Lett* 48(5):e2020GL091441